Nucleic Acids Research, 2026, **54**, gkag426
https://doi.org/10.1093/nar/gkag426
Nucleic Acid Therapeutics

Development of a tetracycline-inducible programmed ribosomal frameshifting platform for sensitive regulation of mammalian gene expression

Sıla Köse [1,2], Elisabeth Müller [1,2], Pierre Gommeringer [1,2,3], Dirk M. Nettelbeck[3], Guy Ungerechts[3,4], Jörg S. Hartig [1,2,*]

[1]Department of Chemistry, University of Konstanz, Konstanz 78457, Germany
[2]Konstanz Research School Chemical Biology, University of Konstanz, Konstanz 78457, Germany
[3]Clinical Cooperation Unit Virotherapy, German Cancer Research Center (DKFZ), Heidelberg 69120, Germany
[4]Department of Medical Oncology, Heidelberg University Hospital, National Center for Tumor Diseases, Heidelberg 69120, Germany
*To whom correspondence should be addressed. Email: joerg.hartig@uni-konstanz.de

Abstract

Developing engineered genetic switches that can respond to specific stimuli in mammalian systems has great potential to advance next-generation therapies. This study introduces a novel tetracycline-inducible artificial riboswitch that regulates gene expression at the translational level via a modified −1 programmed ribosomal frameshifting (−1 PRF) platform. Our dose-response analysis reveals an EC_{50} of 0.41 μM, indicating exceptional sensitivity compared to other tetracycline-dependent artificial riboswitches developed for mammalian applications. By varying the precise spacing and composition of the tetracycline aptamer as the stimulatory structure on the −1 PRF platform, a series of switches has been constructed that enable robust induction of gene expression upon ligand addition. To attain a translational gene control platform with broader applicability, we developed a concept that allows it to be integrated upstream of a gene of interest (GOI), enabling precise control without requiring extensive re-engineering and expressing the GOI as a fusion protein. We validate the platform's effectiveness in several genetic contexts, confirming its modularity. As optimization efforts continue to develop artificial riboswitches with optimized properties in mammalian systems, our findings contribute to the development of highly sensitive and efficient regulatory devices with beneficial characteristics, such as reversibility, modularity, and compatibility with RNA-based delivery therapies.

Graphical abstract

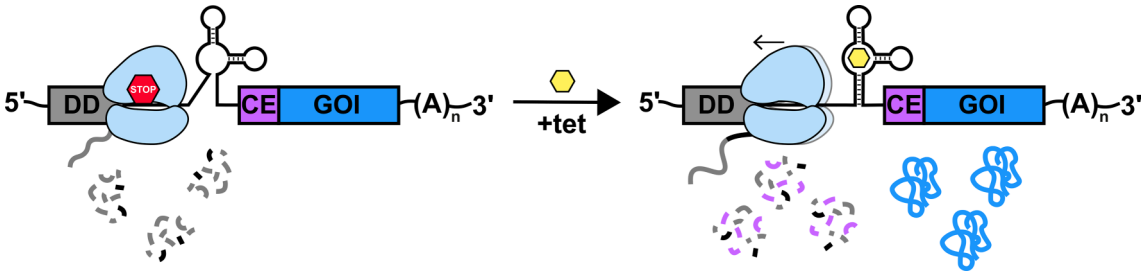

Introduction

In recent years, gene and cell therapies have had a substantial impact on the clinical field by targeting the genetic and molecular drivers of diseases that were previously considered incurable. These treatments have predominantly centered on enhancing and optimizing delivery mechanisms, demonstrating notable clinical efficacy in cases of chronic leukemia [1], spinal muscular atrophy [2], hemophilia [3], cerebral adrenoleukodystrophy [4], β-Thalassemia [5], and inherited retinal dystrophy [6]. Early gene therapy strategies used relatively simple approaches that did not require spatiotemporal control over the therapeutic gene expression. Yet most diseases are complex and dynamic, and most proteins have a narrow therapeutic window [7]. As more complex illnesses are addressed, it is vital to include additional components to regulate the degree and timing of transgene expression in gene therapies. In addition, the ability to regulate both the quantity and timing of the therapeutic cargo would not only promote the broader acceptance of cell and gene treatments but also address the safety and efficacy concerns associated with previous therapies [8–10]. Synthetic gene regulation processes are also extensively utilized in fundamental research to examine

Received: September 8, 2025. **Revised:** March 31, 2026. **Accepted:** April 15, 2026

gene function and signaling networks, as well as to alter gene expression in cellular models in real time [11, 12].

The majority of recent advancements in gene regulation systems that address this gap principally rely on the regulation of transcription utilizing transcriptional effectors. While these systems have been extensively employed in cell culture and animal models due to their excellent dynamic range [13, 14], no approved clinical gene therapies employ foreign proteins as regulatory elements due to the risk of triggering cellular and humoral immune responses and plummeting target gene expression in the long term [15, 16]. In addition to occupying valuable vector genome space, transcription factor-based systems are subject to imperfect regulation and exhibit "leakiness." These issues are particularly pronounced in contexts involving high copy numbers, such as high-titer viral transduction strategies or during replication of oncolytic viral genomes [17–19]. In this aspect, numerous RNA-based regulation systems, such as artificial riboswitches that modulate gene expression as *cis*-regulatory elements, have been developed [20–24]. Riboswitches are allosterically active RNA structures that govern co- and/or post-transcriptional mechanisms by binding to specific ligands via their aptamer domain, which leads to a conformational change in their expression platform [25]. The exploitation of the modular and compact nature of these tools, which are predominantly bacterial in origin, has led to the development of artificial riboswitches that control various co- and/or post-transcriptional mechanisms in mammalian [26–34]. Considerable progress has been achieved, including validation in preclinical models and proof of principle in high-copy contexts, such as self-replicating viral or RNA systems, as demonstrated in studies by Ketzer *et al*. [35, 36]. Nonetheless, transforming these systems into clinical applications remains challenging due to high noise-to-signal ratios and narrow dynamic ranges. Another limitation is the difficulty in achieving effective concentrations of the small molecules to activate the developed switches *in vivo* [37, 38], which is often due to issues such as toxicity or poor bioavailability in most tissues [39, 40].

The development of more sensitive and efficient small molecule-responsive artificial riboswitches faces challenges due to the narrow range of appropriate ligands and the lack of systems refined for medical applications. Despite these obstacles, the tetracycline aptamer has emerged as a notable exception. Initially identified through SELEX in 2001 [41], the tetracycline aptamer has been one of the most extensively employed sensory domains in artificial riboswitches due to its particular promise in addressing these issues. Tetracycline, a small-molecule pharmaceutical, is generally regarded as relatively non-toxic and cell-permeable [42]. The affinity of the tetracycline aptamer for this ligand is remarkable, with a dissociation constant (K_d) of 0.8 nM [43]. Furthermore, the functionality of the developed tetracycline riboswitches has been demonstrated in various organisms [29, 44]. For instance, a recent report by Luo *et al*. [30] describes a tetracycline-responsive system based on polyA signal modulation and alternative splicing in the 5′-UTR. The developed switches Y362 and Y387, with EC_{50} values of ∼0.7 and 0.5 μg/ml [30], respectively, are reported to be suitable for the FDA-approved range of 1 to 5 μg/ml of tetracycline, which is reached after oral dosing at 500 μg twice daily [45].

Artificial riboswitch platforms, such as those that regulate splicing, require themselves and their triggers to be transported into the nucleus. This necessity excludes application opportunities in therapies primarily targeting the cytoplasm, including options that employ RNA viruses [46, 47]. Further constraints arise from the range of inducer signals that cross the nuclear envelope, limiting the suitable choices of inducers [48]. In contrast, artificial riboswitches that utilize expression platforms operating at the translational level are not constrained by such limitations and offer a more rapid response to external stimuli [49]. Typically, artificial riboswitches that regulate translation in mammalian cells focus on the initiation step, similar to their bacterial counterparts; however, they have not yet achieved the same efficacy [50]. This discrepancy arises from the fact that the level of regulation on eukaryotic translation is more complex and requires cooperation from a large set of initiation factors [51]. Instead, we sought to exploit one of the well-studied translational recoding mechanisms, programmed ribosomal frameshifting (PRF), since these mechanisms primarily rely on recognizing conserved *cis*-acting messenger RNA (mRNA) signals or structures to reprogram the ribosome's behavior [52].

As a form of non-canonical translation, PRF enables the production of alternative proteins from a single mRNA by allowing ribosomes to deviate from the original translation frame [53]. Triggered by a variety of cues on the nascent mRNA chain [54, 55], PRF most commonly requires a heptameric "slippery" sequence and a stimulatory secondary structure, generally in the form of a pseudoknot positioned downstream [56–58]. During translation, the increased dwell time required to unwind the stimulatory secondary structure halts the ribosome at the slippery sequence, allowing for the rearrangement of codon-anticodon base pairs in the A and P sites of the ribosome, which shifts the reading frame by 1 or 2 nt [57, 59, 60]. The fact that this process can precisely regulate target gene expression at the translational level by altering the reading frame makes −1 PRF an attractive expression platform for artificial riboswitches. Several attempts have established that pseudoknot-forming aptamers, such as the S-adenosylhomocysteine aptamer [61] and the 7-aminomethyl-7-deazaguanine (preQ1) aptamer [34], can be employed to stimulate frameshifting in a ligand-dependent manner. The latter studies have built upon this foundation by integrating aptamers that control the folding of attenuator hairpins or stimulatory structures [38, 62]. Moreover, stimulatory structures of −1 PRF were modified to be targetable by specific synthetic molecules [63].

Although the ligand-bound form of the tetracycline aptamer contains a non-canonical pseudoknot in its binding pocket [64], no studies have examined its potential as an inducible stimulatory element for −1 PRF. Furthermore, there are still limitations in achieving efficient induction levels and wide dynamic ranges for inducible −1 PRF systems. Moreover, the broad applicability across different genetic contexts may be constrained by the inherent properties of the −1 PRF mechanism, and the lack of small-molecule triggers optimized for clinical use, which present challenges in this regard [38, 65, 66]. Therefore, while advancements have been made in ligand-inducible PRF systems, the aforementioned challenges must be overcome to enable their use in next-generation therapies.

This study presents a novel mammalian riboswitch platform that is modularly attachable upstream of any gene of interest (GOI). Considering potential applications in patients, treatment efficacy, and safety, we chose tetracycline and its aptamer for developing ligand-inducible −1 PRF platforms

[45, 67, 68]. We show that the tetracycline-inducible −1 PRF platform has improved characteristics at ligand concentrations that fall into the clinically approved window [45, 69], spans a wide dynamic range, and shows higher performance in its ON state. The inducible −1 PRF platform's modular design provides a more streamlined and effective approach to gene regulation at the translational level. The engineered platform addresses the issue of co-expressing the GOI as a fusion protein by utilizing cleavage elements. Moreover, a degradation domain (DD) integrated into the platform prevents the accumulation of translational byproducts, including elements of the switch itself. Our findings should prove useful for sophisticated genetic engineering applications in research and medicine where precise control over gene expression is crucial.

Materials and methods

Plasmid construction

psiCHECK™-2 vector (Promega) was used for the dual luciferase reporter assays. This vector carries a firefly luciferase (*hluc+*) gene and a *Renilla* luciferase (*hRluc*) gene. DNA sequence encoding for the single-chain murine interleukin-12 (mIL-12) was constructed by linking complementary DNA (cDNA) sequences of the p35 and p40 subunits with a flexible linker $(Gly_4\ Ser)_3$ sequence described by Veinalde *et al.* (2017) and kindly provided by Prof. Guy Ungerechts [70]. The DD (UbVR) sequence described by Chassin *et al.* (2019) [71] was synthesized by TwistBiosciences (US). The DD-TMEV-RS-2A and the DD-TMEV-INFC-2A modules were inserted upstream of EGFP on the pcDNA5-EGFP-mCherry reporter plasmid via Gibson Assembly for the fluorescence reporter assays. The constructs were created using overhang extension polymerase chain reaction (PCR), followed by ligation with the Quick Ligation™ Kit (NEB) or the Gibson assembly of PCR-amplified vector backbones and inserts in 2× Gibson Assembly Master Mix (NEB). All oligonucleotides were ordered from Sigma–Aldrich. Plasmids were purified using a Zyppy Plasmid Miniprep kit (Zymo Research). Plasmids were verified by sequencing (Eurofins Geomic GmbH or Azenta). All nucleotide sequences that correspond to the −1 PRF platform elements and variants, as described in the main text, are listed in Supplementary Table S1.

Cell culture, transient transfection, and dual-luciferase reporter assay

HeLa, HEK293T, and H1299 cells were cultured in Dulbecco's Modified Eagle's Medium (DMEM, Gibco DMEM, Fisher Scientific) supplemented with 10% (v/v) fetal calf serum and 1% (v/v) penicillin/streptomycin (Fisher Scientific). Cells were maintained at 37°C in a humidified atmosphere with 5% CO_2. Cells were passaged every 2–3 days, and cells older than passage 40 were not used in experiments.

One day before transfection, cells were seeded into 96-well plates at a density of 8×10^3 cells per well. Transfection was performed using Lipofectamine® 3000 (Thermo Fisher Scientific) following the manufacturer's protocol with 100 ng of plasmid DNA per well. After a 4–6 h incubation, the medium was replaced with fresh DMEM, with or without the indicated amount of tetracycline (Merck). For the time-dependent response measurements, incubation was extended overnight.

Eighteen hours after medium replacement, luciferase activity was measured using the Dual-Luciferase® Reporter Assay System (Promega) according to the manufacturer's instructions. Luminescence was quantified using a Spark® multimode microplate reader (Tecan), with a settling time of 0 ms and an integration time of 2000 ms. The luciferase expression from the unmodified transcription unit was used as the internal control for calculating the normalized luciferase gene expression. The relative luciferase activities were calculated following normalization and stated as a percentage of the luciferase activity measured in the unmodified psiCHECK™-2 vector. Similarly, −1 PRF efficiencies were calculated following normalization and stated as a percentage of the luciferase activity measured in the in-frame control (INFC) of the respective −1 PRF module. Luciferase activities were measured as described at the indicated time points for the time-dependent response measurements. Results were reported as mean values with standard deviations of three independent measurements. Unless otherwise stated, all dual-luciferase assays were conducted in HeLa cells.

Fluorescence reporter assay

Transient transfection and tetracycline induction steps were performed in HeLa cells as described. After an 18-h incubation period following the medium change, the cells were rinsed with phosphate buffered saline (PBS), and each well was filled with 100 µl of fresh PBS. Fluorescence readouts were performed using a Spark® multimode microplate reader (Tecan). EGFP fluorescence was detected at an excitation of 478 nm and an emission of 524 nm, with a bandwidth of 20 nm, whereas mCherry was measured at an excitation of 568 nm and an emission of 620 nm, with a bandwidth of 20 nm. To account for background fluorescence, the measured values from non-transfected cells were subtracted from both EGFP and mCherry values. To compensate for variations in transfection efficiency and cell number, the unmodified transcription unit expressing mCherry was used as the internal control for calculating the normalized EGFP gene expression. The relative fluorescence intensities were calculated following normalization and stated as a percentage of the fluorescence intensity measured in the unmodified pcDNA5-EGFP-mCherry vector. The reported data represent the mean of three independent experiments with standard deviation.

ELISA

HeLa cells were seeded at 8×10^3 cells per well in 96-well plates 1 day before transfection. Transfection and induction with tetracycline were carried out as described earlier. After 22 h, culture supernatants were harvested, and the concentration of mIL-12 was determined by sandwich ELISA, according to the manufacturer's instructions (Catalog Number: 88-7121-88, Thermo Fisher Scientific). While the samples were transferred to a 96-well plate precoated with anti-mouse IL-12 antibody and subsequently blocked, the positive control and test samples were diluted in PBS (1:40 and 1:5, respectively). The color reaction was stopped with 100 µl of 2N H_2SO_4, and the optical densities at 450 and 570 nm were quantified using a Spark® multimode microplate reader (Tecan). The values at 570 nm were subtracted from those at 450 nm prior to data analysis. Three technical replicates for each tested tetracycline concentration were assessed in each biologic replicate. Technical replicates with signal levels lower than those of the blank

wells were set to zero. A total of two replicates (one technical replicate of 0 μM tetracycline and one technical replicate of 0.4 μM of tetracycline) were set to zero. Results were reported as mean values with standard deviations of the three independent measurements.

Data analysis

The normalized data were analyzed with two-way analysis of variance in GraphPad Prism software (version 8.3, GraphPad Software, San Diego, CA, USA) ($P \leq .05$, $P \leq .01$, $P \leq .001$, and $P \leq .0001$ were shown as "*", "**", "***", and "****", respectively). Dose-response curves were plotted using GraphPad Prism software (version 8.3, GraphPad Software, San Diego, CA, USA). The data were fitted to a sigmoidal dose-response curve using the "[Agonist] versus response – Three parameters" equation. This model assumes a standard Hill slope of 1.0 and fits the following equation:

$$Y = Ymin + X * \frac{Ymax - Ymin}{EC_{50} + X}.$$

The concentration of agonist that produces a response halfway between the bottom and top values was calculated from the fitted curves and is reported as EC_{50}.

Results

The ligand-bound form of tetracycline aptamer stimulates −1 PRF in a dual reporter system

To test whether the unique formation of the binding pocket of the tetracycline aptamer can be utilized as a stimulatory secondary structure of -1 PRF, we first adapted the dual-luciferase reporter system of the psiCHECK™-2 vector to facilitate analysis of recoding signals [72, 73]. First, the firefly luciferase gene (*hluc+*) was cloned downstream of the *Renilla* luciferase gene (*hRluc*) in −1-frame relative to the start codon of *hRluc*. Next, the respective −1 PRF modules were positioned between the two luciferase genes, with the stop codon for the *hRluc* positioned in the spacer region of the −1 PRF module or marginally downstream in the 0-frame (Fig. 1A). The −1 PRF modules, consisting of a stimulatory signal and a slippery sequence upstream, result in the kinetic partitioning of translating ribosomes, allowing them to continue in different frames at a fixed ratio. Therefore, in this setup, it was expected that ribosomes that undergo a frameshift would yield an entire translated unit, hereafter referred to as a translon, carrying both luciferases as a fusion protein; in contrast, those that do not undergo a frameshift would terminate translation at the stop codon in the spacer region and result in a translon carrying only in *hRluc*.

First, we examined several well-characterized −1 PRF modules in their native setting, i.e. without the tetracycline aptamer (Fig. 1A, upper scheme). The mouse mammary tumor virus (MMTV) [63] and the severe acute respiratory syndrome-related coronavirus 2 (SARS-CoV-2) [74] utilize a pseudoknot (PK) structure as their stimulatory RNA. We also examined Theiler's murine encephalomyelitis virus (TMEV), which uses a trans-acting 2A protein that interacts with a hairpin (HP) structure on the −1 PRF module to stimulate frameshifting [75]. Additionally, we examined human immunodeficiency virus (HIV), which uses an HP structure as its stimulatory RNA, though evidence suggests that it can adopt more elaborate configurations [76–78, 79]. We determined the translation efficiency in the alternative frame relative to the normalized *hluc+* activities measured in cells that carry the unmodified psiCHECK™-2 vector. As different viruses have unique −1 PRF modules to fine-tune the specific ratio of their key viral proteins, the frameshifting efficiencies can vary significantly for each module [80]. Hence, we observed a range between 8.5% and 47% of *hluc+* activity from the different WT −1 PRF modules (Fig. 1B). Since we did not recombinantly express the aforementioned 2A protein in our system [75], we did not observe any frameshifting activity for the WT −1 PRF module of TMEV. Our analysis showed the highest −1 PRF efficiency for SARS-CoV-2-PK, closely followed by HIV-HP.

Subsequently, we developed tetracycline-inducible −1 PRF modules, in which the WT stimulatory secondary structures were substituted with the tetracycline aptamer (Fig. 1A, lower scheme). To compare the −1 PRF efficiencies, we designed all −1 PRF modules to carry a tetracycline aptamer 6 nt downstream of the slippery sequence. This spacer length falls into the typical range observed for native −1 PRF modules with stimulatory pseudoknot structures [81]. Moreover, we restricted the p1 stem of the aptamer to 11 bp for all −1 PRF modules. SARS-CoV-2-RS-6 had the most substantial dynamic range of 6.6-fold. The MMTV-RS-6 also exhibited a similar switching profile, with a slightly lower ON state of 10.5% and a dynamic range of 6.4-fold. Interestingly, this construct exhibited higher −1 PRF activity in its ON state compared to the WT MMTV-PK. Although TMEV-RS-6 had a modest dynamic range of 2.4-fold, the modified spacer length surprisingly resulted in PRF activity induced by tetracycline, even without recombinant 2A protein expression. Notably, this construct exhibits the highest ON-state, at 33.6% (Fig. 1B).

Next, to demonstrate that the rise in *hluc+* levels is due to tetracycline-activated −1 PRF, we designed constructs with impaired −1 PRF elements using TMEV-RS-6 as a representative model and measured their *hluc+* levels. In the first construct, we disrupted the slippery sequence of the tetracycline-inducible TMEV −1 PRF platform to create TMEV-RS-mutSS. Specifically, we replaced the slippery sequence "G-GUU-UUU" with the non-functional sequence "G-AAG-AAG" (Fig. 1C, bottom left panel). The sequence "G-AAG-AAG" does not meet the criteria to be a functional slippery sequence in mammalian cells; therefore, −1 PRF activity is abolished [82]. In a second construct, an "A19U" mutation was introduced in the binding pocket of the tetracycline aptamer to significantly reduce its affinity for tetracycline (Fig. 1C, bottom right panel) [29, 64]. Finally, to measure maximum *hluc+* activity in this setup and calculate the relative −1 PRF efficiencies, we designed a third INFC that has both the mutated slippery sequence and the mutated tetracycline aptamer and positioned the *hluc+* gene in the 0-frame by inserting 1 nt in the spacer region (Fig. 1C, top right panel). Our results showed that mutating the slippery sequence abolished frameshifting, regardless of the presence of tetracycline. Similarly, the mutated tetracycline aptamer did not increase *hluc+* levels in response to tetracycline administration (Fig. 1D). On the contrary, INFC showed higher *hluc+* activity to the unmodified control, indicating that the activity does not get severely affected by the fusion design or the presence of translated −1 PRF elements. The variety in the *hluc+* activities between INFC and the unmodified control psiCHECK™-2 vector could be attributed to their expression

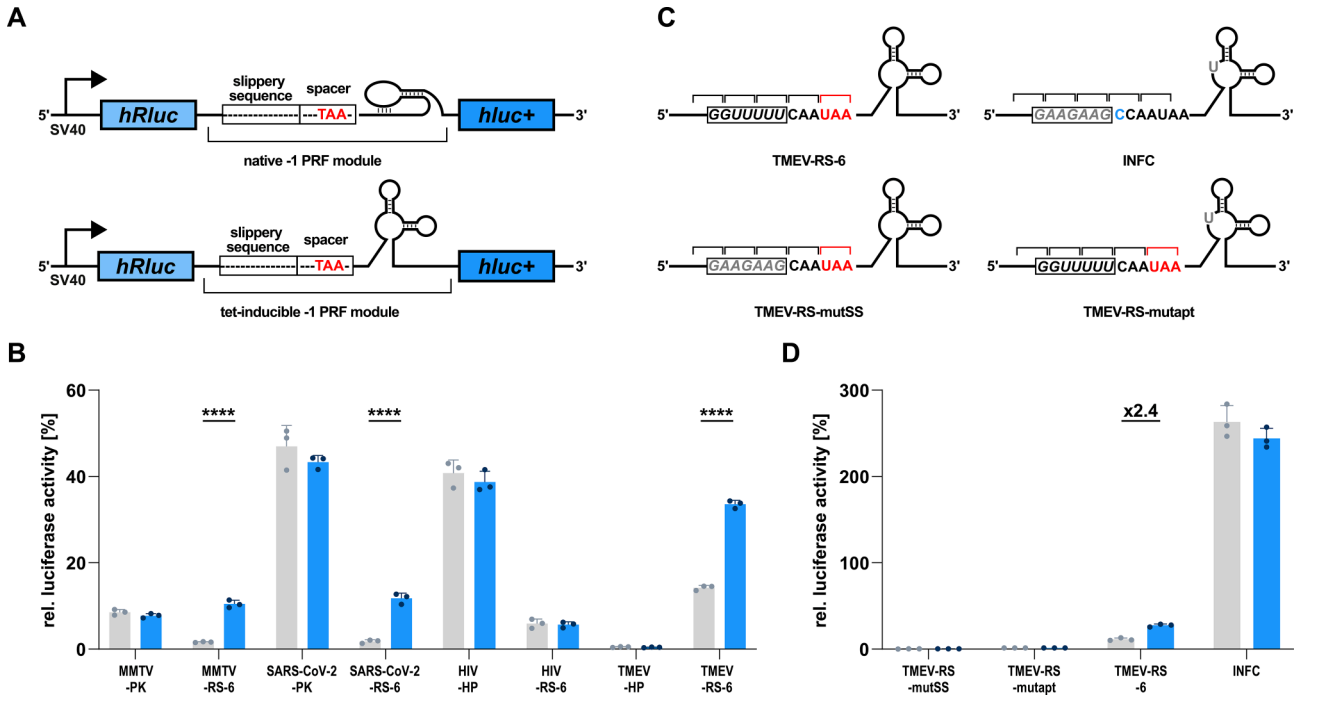

Figure 1. Tetracycline aptamer stimulates −1 PRF when bound to its ligand. (**A**) Top a general scheme of wild-type (WT) −1 PRF modules tested in a dual-luciferase context—*bottom* tetracycline-inducible −1 PRF platform design where the native stimulatory signal is replaced with a tetracycline aptamer. The stop codon in the 0-frame is shown in red. (**B**) Dual-luciferase assay showing the relative *hluc+* activity with no (grey) or 50 μM (blue) tetracycline. MMTV-PK, SARS-CoV-2-PK, HIV-HP, and TMEV-HP represent the natural −1 PRF modules, and MMTV-RS-6, SARS-CoV-2-RS-6, HIV-RS-6, and TMEV-RS-6 represent the tetracycline-inducible −1 PRF modules with a spacer length of 6 nt in the dual-luciferase context. Columns represent the mean ± s.d. of three independent experiments (each with three technical replicates). (**C**) Schematic representation of the constructs used to characterize the tetracycline-inducible −1 PRF platform. TMEV-RS-6 demonstrates the functional tetracycline-inducible TMEV-1 PRF platform. TMEV-RS-mutSS features a mutated slippery sequence, and TMEV-RS-mutapt has a mutated tetracycline aptamer. The INFC is designed to serve as a positive control, carrying a nucleotide insertion at the spacer region and mutated −1 PRF elements. The slippery sequence is in italics; the stop codon is in red; the mutated slippery sequence and the A-U mutation in the tetracycline aptamer are in gray. The inserted nucleotide for the INFC is shown in blue. (**D**) Dual-luciferase assay showing that the relative *hluc+* activity depends on the functionality of the tetracycline-inducible −1 PRF elements. The values above the bars indicate the dynamic range for each respective construct. Columns represent the mean ± s.d. of three independent experiments (each with three technical replicates).

from different transcriptional units. Therefore, the *hluc+* activity of INFC was used to calculate the relative −1 PRF efficiencies in further setups.

In conclusion, the characterization of our initial designs of tetracycline-inducible −1 PRF switches provided promising results, indicating that the translational recoding platform can be an effective alternative to reported artificial riboswitch-controlled gene expression platforms in mammalian cells. We observed switching activities in all tetracycline-inducible −1 PRF modules except HIV-RS-6. In the next chapter, we developed a new approach to fine-tune these activities.

Effects of stability and position of the tetracycline aptamer on −1 PRF efficiency

While the main components of −1 PRF are the slippery sequence and the stimulatory RNA structure, optimal frameshifting also depends on the spacing between these elements. This idea arises from the "tandem-slippage" mechanism of ribosome-bound peptidyl- and aminoacyl-tRNAs when the ribosome reaches the stimulatory RNA structure. At this moment, if the intrinsic activity of the ribosome fails to unwind the stimulatory RNA structure, tension is created in the mRNA. This tension is then released by uncoupling the codon:anticodon complexes and causes an occasional realignment in the −1 frame. As a result, the precise length of the spacer plays a vital role in frameshifting efficiency since it affects the time at which the pseudoknot base is encountered by the active site of the ribosomal helicase to allow frameshifting [81].

Given the impact of the distance between the slippery sequence and the stimulatory RNA structure on modulating translational frameshifting, we next examined a range of alternative designs with the aptamer positioned at various distances from the slippery sequence to determine the most effective layout to increase the number of successful frameshifting events. As variations in spacer length could disrupt the reading frame downstream, we varied the p1 stem length of the aptamer to maintain the downstream −1-frame while avoiding the introduction of premature stop codons through nucleotide substitutions. We started our investigation on the tetracycline-inducible MMTV −1 PRF platform. We varied the length of the spacer from 5 to 8 nt, and the p1 stem lengths of the aptamers span a range of 12–9 bp, respectively (Supplementary Fig. S1). We paid additional attention to the commonly observed spacer lengths of 6 and 7 nt. For these distance alterations, we further examined p1 stem lengths adjusted by ±3 bp, resulting in stem lengths of 8, 11, and 14 bp for the 6-nt spacer and 7, 10, and 13 bp for the 7-nt spacer. This refined approach allowed us to identify changes in the −1 PRF efficiency attributable to adjustments in the stem length of the tetracycline aptamer (Supplementary Fig. S1).

Our results revealed a substantial range in the dynamic ranges of the MMTV-RS module, with observed dynamic ranges spanning from 1.3- to 6.3-fold changes in expression upon addition of tetracycline. Some spacer and stem length combinations resulted in the complete abolition of frameshifting, underscoring the critical importance of precise spacing and stem configuration for functional −1 PRF activity. Additionally, the relative ON states of the riboswitches exhibited significant variability. The relative *hluc+* activities exhibited a range between 1.4% and 10.7%, indicating that specific configurations did not only differ in their dynamic range but also in their absolute expression levels (Supplementary Fig. S1A). Our comparative analysis between different spacer lengths and p1 stems suggests a possible need for a certain level of thermodynamic stability to create resistance to the helicase activity of ribosomes and to induce −1 PRF. However, even though some extended p1 stems favored higher −1 PRF efficiencies, this trend was not universal. In our analysis, the 6-nt spacer with an 11-bp stem exhibited the highest −1 PRF efficiency, followed by the 7-nt spacer with a 10-bp stem. At both spacer lengths, shorter p1 stems have shown six times worse frameshifting efficiency, suggesting higher stability is required for the elevated −1 PRF efficiencies. Still, the longer p1 stems at these fixed spacer lengths did not perform better than their shorter versions. In fact, besides eliminating the dynamic range to negligible levels, longer p1 stem configurations drastically reduced frameshifting efficiency for both ON and OFF states (Supplementary Fig. S1A). Our results highlight the complexity of the interplay between spacer length and stem stability for efficient −1 PRF activity [81, 83]. These findings are consistent with a recent report that proposed the global stability of the stimulatory structure is not directly correlated with frameshifting efficiency, despite its role as a thermodynamic block to translocation [84].

Next, we aimed to improve the tetracycline-inducible TMEV −1 PRF platform by varying the length of the spacer region between the slippery sequence and the downstream tetracycline aptamer (Fig. 2A). Again, we tested varying spacer lengths of 5, 6, and 7 nt to identify the most effective configuration for −1 PRF efficiency. Furthermore, we focused our optimization efforts on modifying the GC content and positioning of G–C base pairs within the p1 stem. The GC content modifications were tested in TMEV-RS-6, which features a 6-nt spacer and an 11-bp p1 stem, and yielded promising initial results. The changes in GC content were designed to fine-tune the stability to improve the structural integrity required for effective frameshifting. These optimization efforts demonstrated that such alterations result in dynamic ranges varying from 2.4 to 9.6-fold change (Fig. 2A). For instance, TMEV-RS-6.1, which had a single G–C to A–U substitution compared to TMEV-RS-6, exhibited the most extensive dynamic range of 9.6-fold. Notably, a single base-pair substitution (G–C to A–U) between variants TMEV-RS-6.1 and TMEV-RS-6.2 resulted in signal levels differing by >90% in the ON state (Fig. 2A). These results suggest that the stem composition and the stability of the base pairs at the entrance channel of the p1 stem of the tetracycline aptamer, where the ribosome encounters first, can significantly impact the −1 PRF efficiency. Moreover, TMEV-RS-6.3, which had the same GC composition as TMEV-RS-6, with one G–C base-pair moved toward the closing end of the joining region of the aptamer, showed the highest ON-state levels. However, it also showed a narrower dynamic range compared to TMEV-RS-6.1, with around five-fold due to its higher background levels (Fig. 2A).

Finally, for the SARS-CoV2-RS, we narrowed our approach. We continued our investigation by specifically varying only the number of G–C base pairs and their positions on the p1 stem of the tetracycline aptamer, without altering the lengths of the p1 stem or spacer. Here, our modification efforts resulted in the construct SARS-CoV2-RS-6.2, which showed *hluc+* activity of ∼15% with a 7.8-fold dynamic range (Supplementary Fig. S1B). These findings continue to underscore the importance of not only the length of the spacer region but also the precise arrangement and composition of the stem structure in optimizing −1 PRF efficiency. By systematically varying these parameters, we identified configurations that maximize the dynamic range and enhance the absolute −1 PRF efficiency levels.

Although our results do not support such an effect, previous studies have reported that changes in spacer length can alter the −1/−2 frameshifting balance [85]. This aspect should be considered when modifying −1 PRF elements.

To evaluate the robustness and versatility of our platform, we also assessed the performance of the TMEV-RS variants in HEK293T and H1299 cell lines. The data indicated that the dynamic ranges of the switches were largely preserved across different cell lines, particularly those with high overall expression levels (Fig. 2A and Supplementary Fig. S2). Though the switches demonstrated consistent dynamic ranges across the tested cell lines, considerable variability was observed in their expression levels, which is consistent with previous reports [86]. The highest and lowest overall expression levels were observed in H1299 and HeLa cells, respectively. The lowest dynamic ranges were observed in HEK293T cells. Notably, TMEV-RS-6.1 exhibited the highest dynamic range across all cell lines, reaching 6.1 in HEK293T cells, 8.6-fold in H1299 cells, and 9.6-fold in HeLa cells. Additionally, TMEV-RS-6.3 demonstrated the highest expression levels in H1299 cells, exceeding 50% ON-state (Supplementary Fig. S2). However, as detailed below, the high-expression phenotype of TMEV-RS-6.3 largely disappeared when implemented in the autonomous design. This indicates that the apparent "high expression" depends heavily on the specific fusion setup rather than being an intrinsic property of the module itself. Depending on the specific application requirements, the desired TMEV-RS variant in the desired cell line can be utilized.

Increased tetracycline sensitivity of the −1 PRF switch

To evaluate the operational range of the developed translational recoding system, we examined the concentration-dependent induction of gene expression by tetracycline in HeLa cells for TMEV-RS-6.1. This analysis revealed an exceptionally low EC_{50} of 0.41 μM (Fig. 2B). This level of sensitivity is noteworthy among previously developed artificial riboswitches operating in mammalian systems [27–29]. In summary, our findings demonstrate the high responsiveness and tunability of the tetracycline-inducible −1 PRF platform, highlighting its potential for translation into practical, real-world applications, including therapeutic contexts such as controlling and dosing targeted cancer therapies, and regenerative medicines. Following the performance evaluation and optimization studies on the tetracycline-inducible −1 PRF platform, the variant TMEV-RS-6.1 was selected for all subse-

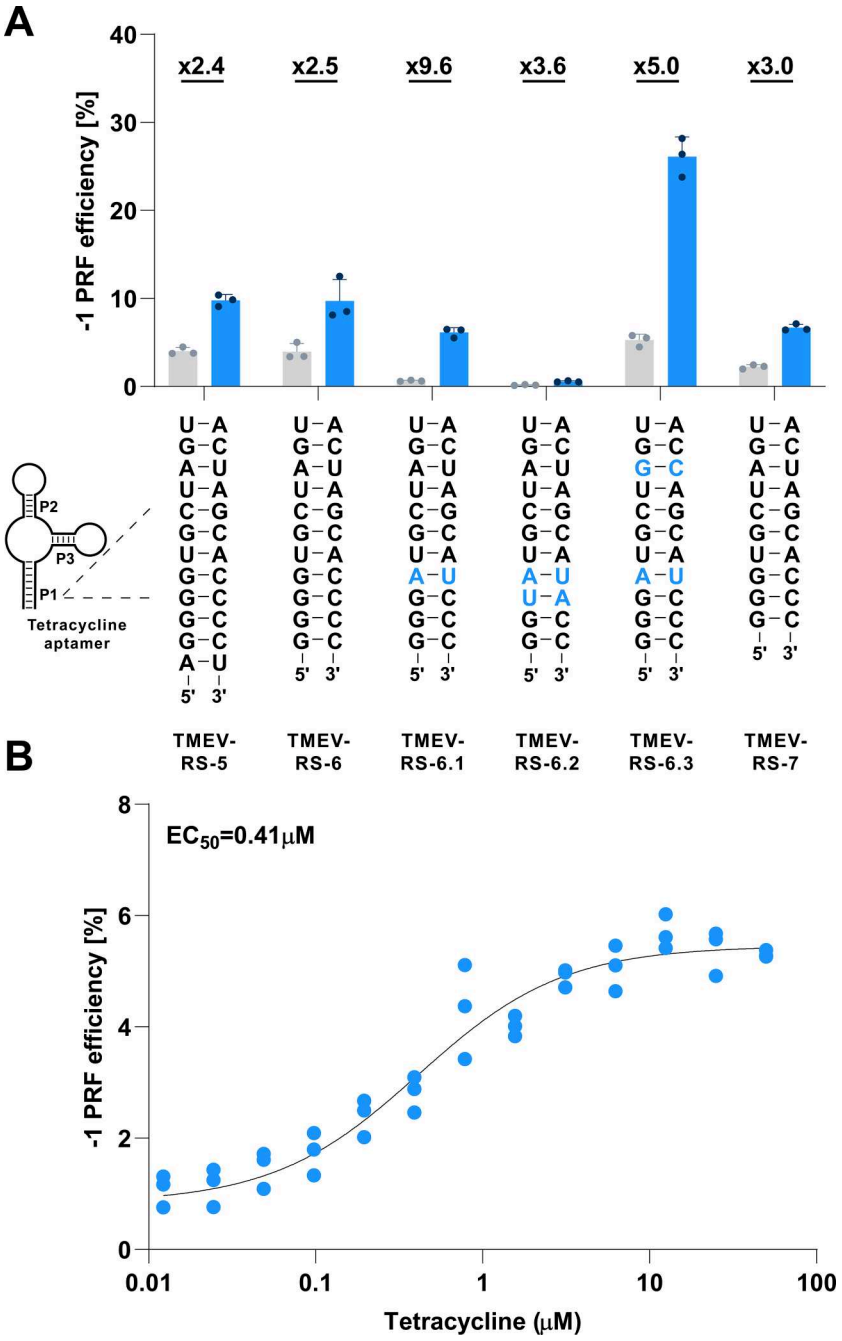

Figure 2. The p1 stem stability and the position of tetracycline aptamer affect the −1 PRF efficiency. (**A**) Dual-luciferase assay showing the effects of spacer/p1 stem variations in the tetracycline-inducible −1 PRF platform with no (grey) or 50 μM (blue) tetracycline. The values above the bars indicate the dynamic range for each respective construct. The corresponding sequences of the p1 stem are presented below the plot, and the spacer length is specified in the construct names (e.g. TMEV-RS-5 indicates a spacer length of 5 nt). Sequential differences between the constructs with the same stem and spacer length are shown in blue. Columns represent the mean ± s.d. of three independent experiments (each with three technical replicates). (**B**) Dose-dependent −1 PRF efficiency of the construct TMEV-RS-6.1. The curve is plotted relative to the INFC expression levels. The concentration corresponding to the half-maximal response (EC_{50}) is indicated on the graph. The data represented show three independent experiments (each with three technical replicates).

quent experiments on the basis of its superior dynamic range, unless specifically stated otherwise.

Autonomous transgene expression controlled by tetracycline-inducible −1 PRF platform

−1 PRF and other translational recoding mechanisms occur during the elongation phase of translation. Consequently, the functionality of these mechanisms is contingent upon the expression of an upstream ORF. Moreover, when the −1 PRF is activated, the translon is expressed as a fusion with the upstream region. In such configurations, the genomic context surrounding the platform and the platform itself can influence each other. This complex behavior challenges the straightforward incorporation of inducible −1 PRF platforms for modular and universal applications regulating transgene expres-

sion, irrespective of the chosen gene, in different cell types or settings. To refine the final translon, we introduced cleavage elements between the −1 PRF platform and the GOI.

In this regard, 2A peptides were considered the primary option [87]. 2A peptides exert their function by impeding the formation of a glycyl-prolyl peptide bond at their C-terminus while maintaining the integrity of the downstream ribosomal elongation process. This unique skipping mechanism results in two separate polypeptide chains where the downstream product only carries an additional proline residue at its N-terminus [88]. We chose 2A peptides due to their compact structure, high cleavage efficiency, and extensive applications in the co-expression of proteins in research and biotechnology settings. Furthermore, by not relying on a *trans*-acting element and displaying a high cleavage efficiency, 2A peptides are ideally suited for developing a versatile, modular platform that can be utilized in different settings.

As a first step, the 2A peptide from the equine rhinitis A virus (E2A) was integrated between TMEV-RS-6.1 and the *hluc*+ gene in the −1 frame [87] (Fig. 3A). In a second configuration, the foot-and-mouth disease virus 2A peptide (F2A) was added downstream of the *hRluc* gene to facilitate the release of both luciferases [89]. Our results show that the tetracycline-inducible −1 PRF platform retained its switching capacity following the integration of 2A peptides, producing similar results to those achieved with the fusion design (Fig. 3B). Notably, incorporating the E2A peptide increased the overall levels of *hluc*+ activity and showed an increase of up to 26.7% in the ON state. However, the increase in expression was accompanied by a slight reduction in the dynamic range due to the higher elevation rates observed in the OFF state. Conversely, introducing the secondary 2A peptide upstream of the tetracycline-inducible −1 PRF platform resulted in a lower ON state and narrower dynamic range compared to the construct carrying a single 2A peptide. The increased number of ribosomal fall-off events during translation is a previously reported drawback of the ribosomal skipping mechanism, which could be a potential outcome with the inclusion of two 2A peptides on a single mRNA [87, 90].

As a next step, we explored the fusion of ubiquitin (Ub) as an alternative cleavage element. Although ubiquitin is a less well-known alternative to 2A peptides, previous studies have demonstrated its effectiveness as a cleavage element when linked to the N-terminus of a protein of interest (POI) This process relies on the recognition of the C-terminal isopeptidase site of the N-linked ubiquitin residue and its subsequent cleavage by deubiquitinating enzymes, thereby leaving the N-terminus of the downstream protein unaltered [91, 92]. In parallel with the 2A peptide-integrated versions, a modified L48R ubiquitin domain, which has been modified to prevent polyubiquitination [93], was directly fused in the −1-frame to the N-terminal region of the *hluc*+ gene to assess its impact on switching capacity. Our findings indicate that Ub is a viable alternative as a cleavage element and shows no interference with the switching activity of the platform (Fig. 3B). While the dynamic range is slightly narrower than the fusion construct, the results show even a higher ON state of 33.1%, and the element offers the advantage of producing a more native version of POI.

In summary, the use of these specific cleavage elements enhances the modularity of our system by yielding POI as a separate protein. The higher levels of −1 PRF efficiency observed in constructs that carry cleavage elements also suggest that this approach could be more effective in accurately quantifying the −1 PRF efficiency. Prior studies have shown that fused reporters may compromise the reliability of signal measurements by affecting the activity of the downstream reporter. Cleavage elements have been recommended when studying translational recoding elements [94, 95].

Controlling the expression of different genes by tetracycline-inducible −1 PRF platform

To achieve a fully autonomous tetracycline-inducible −1 PRF platform that does not rely on the production of the upstream (0-frame) product, we substituted the upstream gene with an N-terminal DD (Fig. 4A). The rationale behind this selection was to employ it as a "stuffer" fragment to maintain the translational context for frameshifting and mitigate the accumulated translated byproducts of the platform. We selected a modified ubiquitin domain (UbVR) with mutations at its C-terminus to inhibit cleavage by isopeptidases [71]. With this tetracycline-inducible PRF setup, the DD-linked 0-frame-encoded translon is always subject to targeted proteasomal degradation, as it is translated irrespective of ligand presence. Conversely, with successful −1 PRF induced by tetracycline, the cleavage element (e.g. 2A or Ub, see above) separates the target protein from the translated byproduct, thereby preventing its degradation.

To assess the modularity of our newly autonomous design, we integrated the autonomous tetracycline-inducible −1 PRF platform based on TMEV-RS-6.1 into the upstream region of the *hluc*+ and *hRluc* transcription units. As each luciferase serves as a distinct reporter within its circuit in the dual-luciferase system, this allowed us to evaluate the operational characteristics of the platform in each transcription unit. Initially, both versions of the platform carrying a 2A peptide or Ub were tested upstream of *hluc*+, positioned downstream of the HSV-TK promoter. Subsequently, both versions with different cleavage elements were also cloned upstream of the *hRluc* gene, directed by the SV40 early enhancer/promoter in the psiCHECK™-2 vector. Our results showed moderate variation in switch performance between these two distinct genetic setups. Specifically, when the platform was used to regulate *hRluc* expression, its performance was superior to the case where it controlled *hluc*+ expression.

When regulating *hRluc* expression, the autonomous tetracycline-inducible −1 PRF platform with the Ub domain yielded the highest dynamic range of 11.1-fold (Fig. 4B, right panel). Here, the platform with the 2A peptide showed the highest ON-state and a dynamic range of around 8.2-fold. Conversely, when regulating *hluc*+ expression, the platform with 2A peptide showed its highest ON-state and the dynamic range of six-fold (Fig. 4B, left panel). While this comparative analysis revealed that the autonomous tetracycline-inducible −1 PRF platform maintained its overall switching capabilities in different configurations, it also underscores the importance of the transcriptional machinery and its influence on the overall efficacy of artificial gene regulation systems. Factors such as promoter compatibility can influence the levels and the stability of the transcribed mRNAs. Understanding these interactions would provide critical insights into tailoring the −1 PRF platforms for specific applications based on the inherent characteristics of the transcriptional unit involved.

To test if the high ON-state levels of the TMEV-RS-6.3 variant generalize to the autonomous design, we inserted the

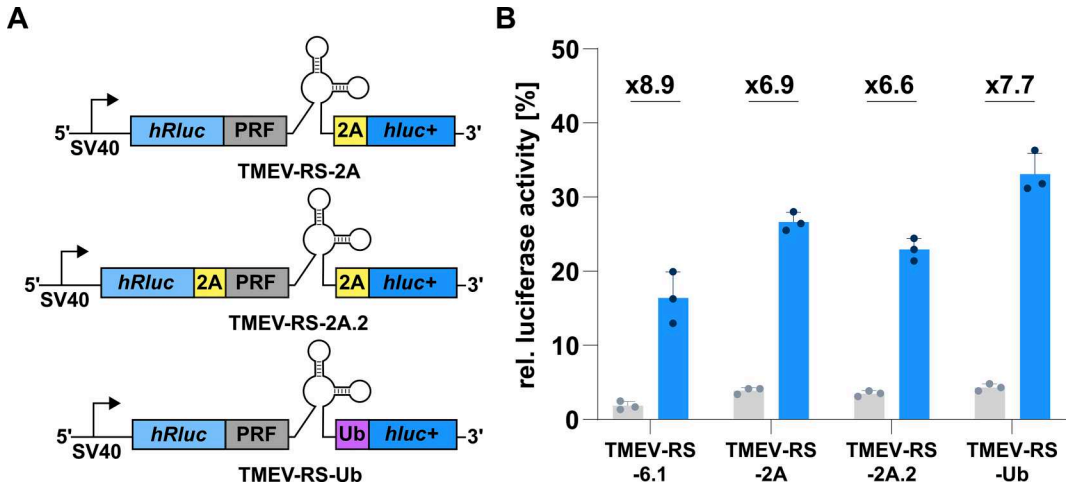

Figure 3. Cleavage elements can be integrated into the tetracycline-inducible −1 PRF platform. (**A**) Schematic representation of the cleavage elements integrated into the tetracycline-inducible −1 PRF platform. An E2A peptide is positioned upstream of the *hluc+* in the −1-frame for the constructs shown at the top and in the middle. An F2A peptide is positioned in the 0-frame upstream of the tetracycline-inducible −1 PRF platform for the construct depicted in the middle. On the bottom construct, ubiquitin (Ub) was placed in the −1-frame upstream of the *hluc+* . (**B**) Dual-luciferase assay showing the impact of the cleavage elements on the −1 PRF efficiency with no (grey) or 50 μM (blue) tetracycline. The values above the bars indicate the dynamic range for each construct. Columns represent the mean ± s.d. of three independent experiments (each with three technical replicates).

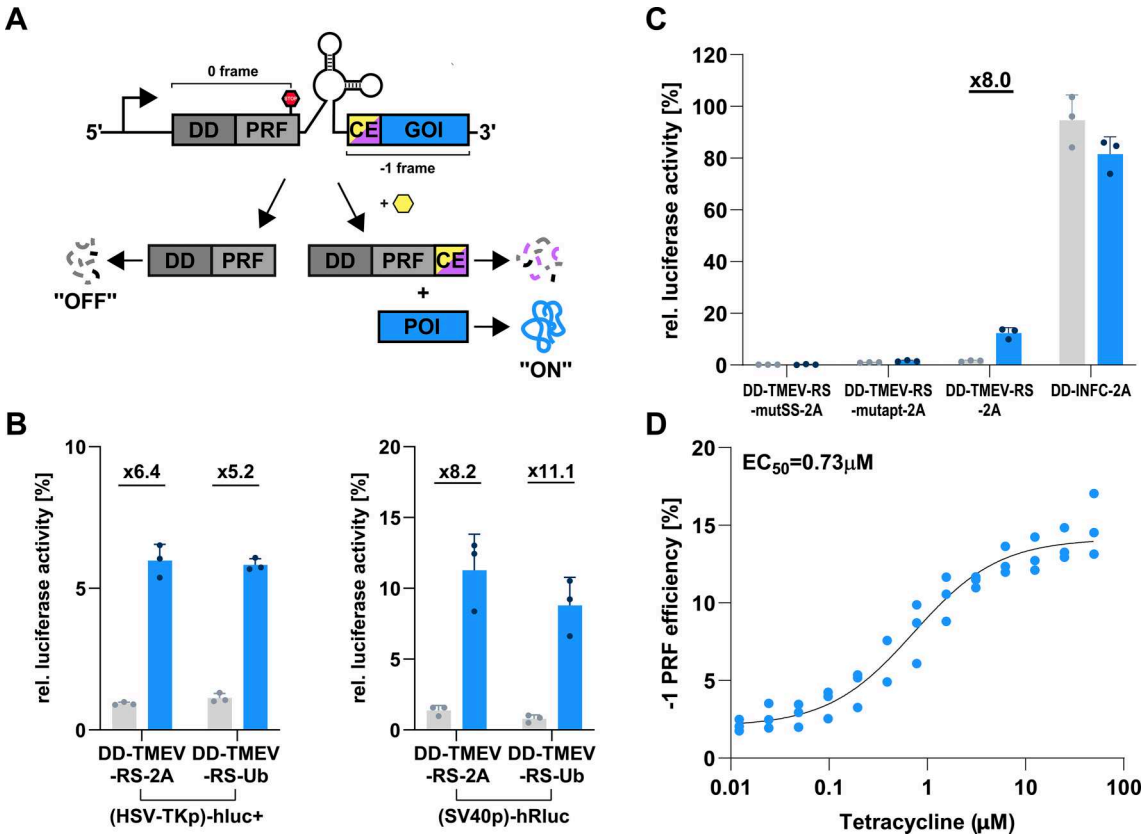

Figure 4. The autonomous tetracycline-inducible −1 PRF platform preserves its switching activity across different transcription units and GOIs. (**A**) General scheme of the autonomous tetracycline-inducible −1 PRF platform. DD represents the non-cleavable Ub, followed by a cleavage element, which is either E2A or Ub upstream of GOI. (**B**) Dual-luciferase assay showing relative luciferase activities of the autonomous tetracycline-inducible −1 PRF platform in *hluc+* transcription unit driven by HSV-TK promoter (left panel) and in *hRluc* transcription unit driven by SV40 promoter (right panel) with no (grey) or 50 μM (blue) tetracycline. The numbers above the bars indicate the dynamic range for each construct. Columns represent the mean ± s.d. of three independent experiments (each with three technical replicates). (**C**) The characterization of the autonomous tetracycline-inducible −1 PRF platform in pSV-40-driven *hRluc* transcription unit with no (grey) or 50 μM (blue) tetracycline. As used in the initial characterization, control constructs are DD-TMEV-RS-mutSS-2A, which has a mutated slippery sequence, and DD-TMEV-RS-mutapt-2A, which has a mutated tetracycline aptamer (see Fig. 1C). The INFC named DD-INFC-2A was used in this setup. Columns represent the mean ± s.d. of three independent experiments (each with three technical replicates). (**D**) Dose-dependent luciferase activity of the autonomous tetracycline-inducible −1 PRF platform. The curve is plotted relative to the DD-INFC-2A expression levels. Data represent three independent experiments (each with three technical replicates).

TMEV-RS-6.3 module, carrying a 2A peptide, downstream of the SV40 early enhancer/promoter that drives *hRluc* expression. In this setting, the TMEV-RS-6.3 module no longer exhibited elevated expression; rather, it fell within the range of TMEV-RS-6.1, with a comparably lower dynamic range (Supplementary Fig. S3). This result underscores the context-dependence of its performance in the fusion setting as pointed out in previous studies [94, 95].

Further analysis was conducted to assess whether the functional mechanism or the sensitivity of the tetracycline-inducible −1 PRF platform was affected in the autonomous setting. First, the effect of the N-terminus DD on the expression levels in the autonomous tetracycline-inducible −1 PRF platform was analyzed. Without a cleavage element present, a drop of around 80% was observed in the overall expression levels (Supplementary Fig. S4). Next, the mutational analysis of the −1 PRF components was conducted using the same approach described in Fig. 1B. It was shown that the impaired −1 PRF elements abolish the platform's switching activity, regardless of the presence of tetracycline (Fig. 4C). Moreover, the dose-response measurements indicated that the EC_{50} of the autonomous tetracycline-inducible −1 PRF platform remained consistently low, exhibiting only modest variation from TMEV-RS-6.1 (Fig. 4D).

To further evaluate the broad utility of our autonomous tetracycline-inducible −1 PRF platform across various genetic environments, we aimed to regulate the expression of the EGFP gene driven by the CMV promoter (Supplementary Fig. S5A). In the fluorescence context, the autonomous tetracycline-inducible −1 PRF platform exhibited marginally elevated expression levels, with a more constrained dynamic range of 6.3-fold in comparison to the luciferase context (Fig. 4C and Supplementary Fig. S5B). Despite the heterogeneity in genetic context and assay characteristics, the platform demonstrated consistent response profiles across both reporters, suggesting that its sensitivity remained unaltered. Specifically, the platform achieved a 3.9-fold increase at 0.4 μM tetracycline, which is similar to its 3.2-fold increase observed with 0.39 μM tetracycline in the luciferase context (Fig. 4D and Supplementary Fig. S5B). However, the percentage of relative expression levels determined relative to the INFC construct was notably lower in the EGFP context, with 58%, compared to the luciferase context (over 80%, Fig. 4C and Supplementary Fig. S5B).

Previous comparative analyses of genetic reporter systems have demonstrated that luciferase signals can plateau earlier than fluorescence signals at higher protein expression levels [96]. Therefore, the lower percentage of relative expression levels observed for INFC in the EGFP context can be attributed to the variability in the absolute reporter activity levels measured in the unmodified vectors. Moreover, the lower background and greater fold induction of the platform observed in the luciferase context were potentially due to the suitability of bioluminescence assays for more precise quantification of gene expression [97]. In conclusion, we observed robust switching performances with both reporters.

To test the therapeutic applicability of the autonomous tetracycline-inducible −1 PRF platform in different genetic contexts, we next sought to control the production of the immunostimulatory cytokine, interleukin 12 (IL-12). IL-12 is a potent inducer of T-cell activity. It exhibits significant anticancer properties through its critical role in modulating early non-specific innate resistance and adaptive type 1 T cell-mediated immunity [98, 99]. IL-12 enhances the cytotoxic activities of NK and T cells by promoting their proliferation and the production of IFN-γ, which is central to orchestrating the TH1 immune response [100, 101]. However, the systematic delivery of IL-12 poses a serious challenge due to its severe toxic effects [102]. Therefore, the controlled release of IL-12 is an attractive strategy to minimize associated side effects and enhance local immune responses in the tumor microenvironment in cancer immunotherapy applications [103–105].

First, we replaced the *hluc+* gene of the psiCHECK™-2 vector with the single-chain mIL-12 coding sequence, resulting in a positive control construct that constitutively expresses mIL-12 downstream of the HSV-TK promoter. Then, to achieve mIL-12 expression under the control of the autonomous tetracycline-inducible −1 PRF platform, we integrated the DD-TMEV-RS-2A module upstream of the mIL-12 CDS (Fig. 5A). We performed ELISA assays to quantify secreted mIL-12 levels from the cells transfected with the described constructs. To evaluate whether the timing and magnitude of the therapeutic payload could be regulated with our platform, we performed inductions with varying concentrations of tetracycline. The findings demonstrated that the tetracycline-inducible −1 PRF platform maintained its dynamic range and relative ON/OFF states, aligning closely with results obtained from luciferase assays (Fig. 5B). The background mIL-12 expression level of the tetracycline-inducible −1 PRF platform was remarkably low at ∼0.5% of the positive control. Notably, the switching activity exhibited a dose-dependent increase, reaching expression levels of 1.6% at 0.4 μM tetracycline and 7.4% at 50 μM tetracycline. These results highlight the modularity of the tetracycline-inducible −1 PRF platform and affirm its potential as a valuable tool for precise gene regulation in clinical and research settings.

External elements can optimize the tetracycline-inducible −1 PRF platform

Despite its advances, the −1 PRF systems are constrained because only a fraction of ribosomes adopt the alternative frame, even in the WT −1 PRF setups. Therefore, the expression levels of the tetracycline-inducible −1 PRF platform in the ON state could be suboptimal for specific therapeutic applications. To enhance system performance in the ON state by boosting mRNA half-life and thereby increasing the absolute target protein levels from repeated translation events, we integrated an mRNA-stabilizing element, a MALAT1 element for nuclear expression (ENE), into our system (Supplementary Fig. S6A). This distinctive triple-helix structure, present at the 3′ ends of MALAT1 long noncoding RNAs (lncRNAs), protects the 3′ end of RNA from 3′–5′ exonucleases, even in the absence of poly(A) tails [106]. To emulate this shielding effect on the mRNA from rapid degradation and extend its half-life, we incorporated the MALAT1 ENE triplex [107], followed by an HDV ribozyme [108], into the 3′ untranslated region of our GOI. By adding a ribozyme that cleaves itself, the MALAT1 ENE triplex can accurately form its unique structure without relying on the natural processing of MALAT1 in cells [109, 110]. This improvement in the target mRNA stability enhanced signal levels of the autonomous tetracycline-inducible −1 PRF platform, ∼13.7-fold and 20.1% of expression in the ON state (Supplementary Fig. S6B). Moreover, the dynamic range was increased by approximately two-fold. Consequently, by incorporating different expression-boosting el-

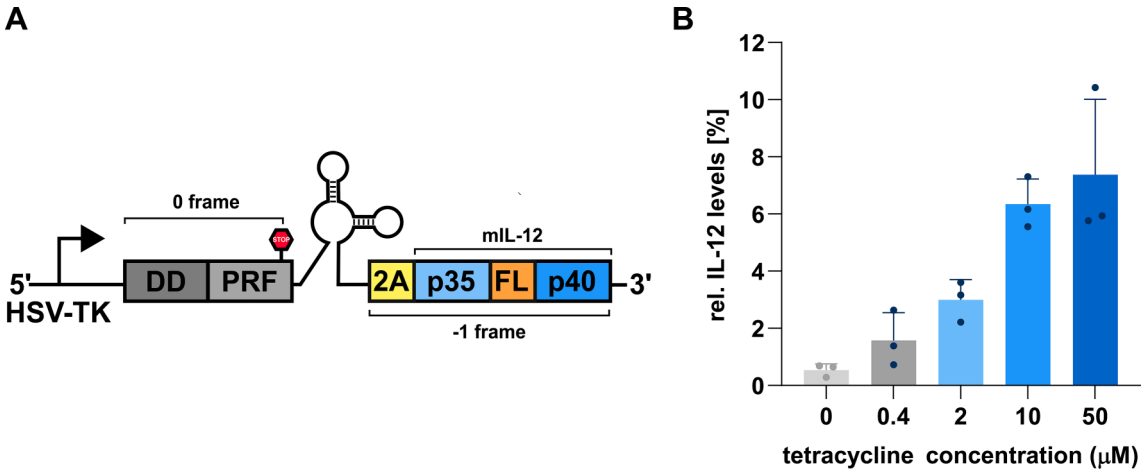

Figure 5. Tetracycline-inducible −1 PRF platform can regulate the timing and the magnitude of mIL-12 expression. (**A**) General scheme of the autonomous tetracycline-inducible −1 PRF platform controlling the expression of single-chain mIL-12. The DD-TMEV-RS-2A module is positioned upstream of the single-chain mIL-12 CDS described above. mIL-12 CDS comprises the p35 subunit (including its 22 aa long signal peptide), followed by $(Gly_4Ser)_3$ flexible linker, and the p40 subunit. (**B**) ELISA assay showing the relative mIL-12 levels measured in the supernatants of HeLa cells carrying the tetracycline-inducible −1 PRF platform or the unregulated mIL-12 (positive control). Cells were induced with tetracycline concentrations as specified. The stated relative mIL-12 levels are the percentages of the mIL-12 levels measured in the respective positive controls induced with the same amount of tetracycline. Columns represent the mean ± s.d. of three independent experiments (each with three technical replicates).

ements with the tetracycline-inducible −1 PRF platform, we showed that it is possible to increase the production of the POI, thereby fulfilling the specific therapeutic requirements of various diseases when needed.

Finally, DLA assays were performed at several designated time points following the addition of tetracycline to evaluate the temporal gene expression of our optimized autonomous tetracycline-inducible −1 PRF platform. A previously reported alternative splicing-based tetracycline switch, Tet9_ex [29], was tested alongside our platform in these assays. The results demonstrated that the optimized tetracycline-inducible −1 PRF platform achieved a consistently higher mean fold change with 10 μM tetracycline and exhibited a more rapid increase over time than Tet9_ex. Remarkably, the optimized tetracycline-inducible −1 PRF platform showed a two-fold increase as early as 1 h post-tetracycline addition, and this effect amplified to reach a 9.1-fold increase after 8 h (Supplementary Fig. S7). These results highlight the rapid response times of our inducible translational reprogramming platform and confirm the robust responsiveness of post-transcriptional gene regulation platforms that act on mature mRNAs [40]. Overall, the presented findings demonstrate that the developed autonomous −1 PRF platform is a modular, versatile, RNA-only tool for conditional control of gene expression. This modularity ensures that the developed platform should be adaptable for diverse applications, potentially providing reliable control over gene expression in various experimental and therapeutic contexts.

Discussion

Translational recoding, particularly −1 PRF, is widely exploited by viruses for gene expression regulation [111, 112]. The use of translational recoding signals as basic circuit components in synthetic biology was previously discussed [113] and −1 PRF has become a valuable tool for synthetic control of gene expression in eukaryotic systems [114, 115]. In this study, we sought to expand this toolbox by developing a tetracycline-inducible mammalian riboswitch that controls gene expression at the translational level. By adapting −1 PRF modules from various viruses and utilizing components from the synthetic biology toolkit, we engineered a modular platform that can be integrated into diverse genetic and cellular environments. Natural and artificial riboswitches typically regulate gene expression by modifying the accessibility of essential gene sequences through metabolite-induced alternative conformations, influencing processes such as transcription termination, translation initiation, and splicing via their expression platform [29, 32, 116]. The formation of these alternative secondary structures depends on how the aptamer domain's occupancy status is transferred to the expression platform, a process that is currently poorly understood [117]. Conversely, in our system, metabolite binding induces pseudoknot formation and structural stabilization of the aptamer domain directly, rather than masking or exposing sequences. This structural stabilization is necessary to trigger the switch, effectively merging the aptamer domain with the expression platform into a unified functional unit. While it remains to be fully determined whether operating as a single entity or another mechanism results in improved sensitivity, our dose-response analysis showed that the tetracycline-inducible −1 PRF platform can respond effectively within the clinically relevant EC_{50} range of the ligand. These findings suggest that the platform ensures efficacy at reduced concentrations of the effector molecule, likely decreasing the potential toxicity associated with high-concentration requirements. Our findings provide preliminary evidence of a direct, robust regulatory capability inherent in the platform that boosts its sensitivity.

In the pharmacokinetic study conducted by Strobel *et al.*, peak plasma concentrations of 42 μM and residual levels of 3.3 μM at the eighth hour were measured following a single intraperitoneal administration of tetracycline at 54 mg/kg in C57Bl/6 mice. Furthermore, exposure levels in various murine organs were evaluated 2 h after tetracycline administration, which revealed total concentrations of 16.4 μM in plasma,

5.7 μM in the lung, 7.8 μM in muscle, 8.0 μM in the heart, 27.2 μM in the kidney, 149 μM in the liver, 0.42 μM in the brain, and 0.88 μM in eyes [40]. In our cellular assays, a tetracycline concentration of 0.39 μM, similar to the concentration measured in the brain, induced a 4.1-fold increase in signal levels with the autonomous tetracycline-inducible −1PRF platform (Fig. 4D). While doses that work in cellular assays may not directly translate to effective doses *in vivo*, the high sensitivity observed in our platform is potentially compatible with therapeutic applications targeting various tissues.

Considering that differences in the transcriptional and translational machinery occur in different cell types, the performance of synthetic gene-regulatory tools can show heterogeneity when operating in other cell lines. Higher switch performance in H1299 and HeLa cells may indicate that the tetracycline-inducible −1 PRF platform exhibits better performance in cancerous cell lines. Nevertheless, further analysis, such as testing additional cell lines, primary cancer cell models, and animal tumor models, is necessary to determine how universally the switches can be applied or which switch variant is most suitable in each context. For instance, trials conducted with TMEV-RS variants in HeLa cells exhibited lower noise signals. In contrast, in H1299 cells, TMEV-RS variants demonstrated much higher overall signal levels.

To further optimize the system toward applicability, we aimed to make the inducible −1 PRF platform modular by introducing an upstream DD and a cleavage element. This autonomous platform prevents the accumulation of translated byproducts and releases the target protein from the byproducts when activated. This design of our system sets it apart from previous inducible −1 PRF platforms, enhancing its adaptability and ease of use in diverse applications. Indeed, our results are consistent with this notion, demonstrating the precise modulation of all four tested target genes, including cytoplasmic and secreted proteins, such as mIL-12. Furthermore, the system remains functional with promoters of varying strengths, allowing for adaptation to different genes or therapeutic needs. Our system's low background and dose-dependent response demonstrate its potential to fine-tune the production of a proof-of-concept therapeutic payload, which is critical for many adaptive therapies targeting complex diseases such as cancer and autoimmune disorders [118, 119].

Additionally, the system's dynamic range is enhanced by modifications to the −1 PRF switch modules, allowing it to regulate gene expression over a broad range of tetracycline concentrations. This flexibility ensures that the system can be tuned to achieve desired protein expression levels tailored to specific therapeutic needs. However, the system is not without limitations. It has been observed that the maximum ON-state achieved in many setups reaches only 30% of the reference expression levels. The lower expression levels may be attributed to the inherent characteristics of −1 PRF, as the stimulatory structure element does not result in the complete adoption of the alternative frame. To address this, introducing or replacing regulatory elements that enhance the mRNA stability could improve overall translation efficiency and expression levels, as demonstrated by the incorporation of the MALAT1 ENE triplex into the 3′ UTR (Supplementary Fig. S6).

The implications of this work are significant, as it advances targeted therapies by precisely controlling gene expression in response to external triggers. In general, synthetic tools that rely on nuclear processes, such as transcriptional effector or splice switches, are not feasible for specific therapeutic strategies, particularly those involving RNA delivery. However, the inducible −1 PRF platform functions in the cytoplasm, making it particularly relevant. Additionally, it maintains its structural integrity during switching, unlike aptazyme switches, allowing for the dynamic modulation of gene expression over extended periods. Although the maximal expression induced by our PRF switches is generally lower than that reported for mammalian aptazymes, their dynamic range falls in a similar range while avoiding the high basal background often reported for aptazymes [27, 28, 31, 120–124]. Furthermore, our PRF switches respond at markedly lower ligand concentrations than aptazyme systems, which often require an inducer concentration of ≥10–100 μM for full regulation [27, 28, 120–124]. In conclusion, compared with previously developed artificial riboswitches, the present system offers a modular tool with reversible and rapid response to its specific cue at the translational level, rendering it a promising instrument for applications in research and medicine.

Acknowledgements

We acknowledge financial support by the Deutsche Forschungsgemeinschaft (DFG, Project A05, CRC 969). The authors thank Astrid Joachimi and Dmitry Galetskyi (University of Konstanz) for their technical assistance, and Vera Hedwig, Martin Scheffner (University of Konstanz), and Laura Kayser (German Cancer Research Center, DKFZ) for their valuable discussions.

Author contributions: Sıla Köse (Conceptualization [lead], Data curation [lead], Formal analysis [lead], Investigation [lead], Methodology [lead], Visualization [lead], Writing – original draft [lead], Writing – review & editing [equal]), Elisabeth Müller (Investigation [supporting], Writing – review & editing [supporting]), Pierre Gommeringer (Investigation [supporting], Writing – review & editing [supporting]), Dirk M. Nettelbeck (Writing – review & editing [supporting]), Guy Ungerechts (Writing – review & editing [supporting]), and Jörg Steffen Hartig (Conceptualization [supporting], Formal analysis [supporting], Funding acquisition [lead], Project administration [lead], Resources [lead], Supervision [lead], Writing – review & editing [equal])

Supplementary data

Supplementary data is available at NAR online.

Conflict of interest

S.K. and J.S.H. are inventors on a patent application that describes parts of this publication. The remaining authors declare no competing interests.

Funding

This work was supported by the Deutsche Forschungsgemeinschaft (DFG) through the Collaborative Research Center SFB 969, "Chemical and Biological Principles of Cellular Proteostasis" (A05), and by the German Cancer Aid (Deutsche Krebshilfe) under grant numbers 70114315 and 70114400 (awarded to D.M.N., J.S.H., and G.U.). Funding to pay the

Open Access publication charges for this article was provided by the University of Konstanz, AG Hartig.

Data availability

Data and materials are available upon request.

References

1. Lim WA, June CH. The principles of engineering immune cells to treat cancer. *Cell* 2017;168:724–40. https://doi.org/10.1016/j.cell.2017.01.016
2. Finkel RS, Mercuri E, Darras BT *et al.* Nusinersen versus sham control in infantile-onset spinal muscular atrophy. *N Engl J Med* 2017;377:1723–32. https://doi.org/10.1056/NEJMoa1702752
3. Nathwani AC, Reiss UM, Tuddenham EG *et al.* Long-term safety and efficacy of factor IX gene therapy in hemophilia B. *N Engl J Med* 2014;371:1994–2004. https://doi.org/10.1056/NEJMoa1407309
4. Eichler F, Duncan C, Musolino PL *et al.* Hematopoietic stem-cell gene therapy for cerebral adrenoleukodystrophy. *N Engl J Med* 2017;377:1630–8. https://doi.org/10.1056/NEJMoa1700554
5. Locatelli F, Thompson AA, Kwiatkowski JL *et al.* Betibeglogene autotemcel gene therapy for non–β0/β0 genotype β-thalassemia. *N Engl J Med* 2022;386:415–27. https://doi.org/10.1056/NEJMoa2113206
6. Russell S, Bennett J, Wellman JA *et al.* Efficacy and safety of voretigene neparvovec (AAV2-hRPE65v2) in patients with RPE65-mediated inherited retinal dystrophy: a randomised, controlled, open-label, phase 3 trial. *The Lancet* 2017;390:849–60. https://doi.org/10.1016/S0140-6736(17)31868-8
7. Clackson T. Regulated gene expression systems. *Gene Ther* 2000;7:120–5. https://doi.org/10.1038/sj.gt.3301120
8. Morgan RA, Yang JC, Kitano M *et al.* Case report of a serious adverse event following the administration of T cells transduced with a chimeric antigen receptor recognizing ERBB2. *Mol Ther* 2010;18:843–51. https://doi.org/10.1038/mt.2010.24
9. Hinderer C, Katz N, Buza EL *et al.* Severe toxicity in nonhuman primates and piglets following high-dose intravenous administration of an adeno-associated virus vector expressing human SMN. *Hum Gene Ther* 2018;29:285–98. https://doi.org/10.1089/hum.2018.015
10. Fitzgerald JC, Weiss SL, Maude SL *et al.* Cytokine release syndrome after chimeric antigen receptor T cell therapy for acute lymphoblastic leukemia. *Crit Care Med* 2017;45:e124–31. https://doi.org/10.1097/CCM.0000000000002053
11. Lienert F, Lohmueller JJ, Garg A *et al.* Synthetic biology in mammalian cells: next generation research tools and therapeutics. *Nat Rev Mol Cell Biol* 2014;15:95–107. https://doi.org/10.1038/nrm3738
12. Bashor CJ, Collins JJ. Understanding biological regulation through synthetic biology. *Annu Rev Biophys* 2018;47:399–423. https://doi.org/10.1146/annurev-biophys-070816-033903
13. Baim SB, Labow MA, Levine AJ *et al.* A chimeric mammalian transactivator based on the lac repressor that is regulated by temperature and isopropyl beta-D-thiogalactopyranoside. *Proc Natl Acad Sci USA* 1991;88:5072–6.
14. Gossen M, Freundlieb S, Bender G *et al.* Transcriptional activation by tetracyclines in mammalian cells. *Science* 1995;268:1766–9. https://doi.org/10.1126/science.7792603
15. Latta-Mahieu M, Rolland M, Caillet C *et al.* Gene transfer of a chimeric trans-activator is immunogenic and results in short-lived transgene expression. *Hum Gene Ther* 2002;13:1611–20. https://doi.org/10.1089/10430340260201707
16. Guiner CL, Stieger K, Snyder RO *et al.* Immune responses to gene product of inducible promoters. *CGT* 2007;7:334–46. https://doi.org/10.2174/156652307782151461
17. Fechner H, Wang X, Srour M *et al.* A novel tetracycline-controlled transactivator–transrepressor system enables external control of oncolytic adenovirus replication. *Gene Ther* 2003;10:1680–90. https://doi.org/10.1038/sj.gt.3302051
18. Fecker LF, Schmude M, Jost S *et al.* Efficient and selective tumor cell lysis and induction of apoptosis in melanoma cells by a conditional replication-competent CD95L adenovirus. *Exp Dermatol* 2010;19:56–66. https://doi.org/10.1111/j.1600-0625.2009.00977.x
19. Rohmer S, Mainka A, Knippertz I *et al.* Insulated hsp70B′ promoter: stringent heat-inducible activity in replication-deficient, but not replication-competent adenoviruses. *J Gene Med* 2008;10:340–54. https://doi.org/10.1002/jgm.1157
20. Wang S, Emery NJ, Liu AP. A novel synthetic toehold switch for microRNA detection in mammalian cells. *ACS Synth Biol* 2019;8:1079–88. https://doi.org/10.1021/acssynbio.8b00530
21. Kaseniit KE, Katz N, Kolber NS *et al.* Modular, programmable RNA sensing using ADAR editing in living cells. *Nat Biotechnol* 2023;41:482–7. https://doi.org/10.1038/s41587-022-01493-x
22. Zhao EM, Mao AS, Puig H *et al.* RNA-responsive elements for eukaryotic translational control. *Nat Biotechnol* 2022;40:539–45. https://doi.org/10.1038/s41587-021-01068-2
23. Gambill L, Staubus A, Mo KW *et al.* A split ribozyme that links detection of a native RNA to orthogonal protein outputs. *Nat Commun* 2023;14:543. https://doi.org/10.1038/s41467-023-36073-3
24. Spöring M, Finke M, Hartig JS. Aptamers in RNA-based switches of gene expression. *Curr Opin Biotechnol* 2020;63:34–40.
25. Winkler WC, Breaker RR. Regulation of bacterial gene expression by riboswitches. *Annu Rev Microbiol* 2005;59:487–517. https://doi.org/10.1146/annurev.micro.59.030804.121336
26. Yen L, Svendsen J, Lee J-S *et al.* Exogenous control of mammalian gene expression through modulation of RNA self-cleavage. *Nature* 2004;431:471–6. https://doi.org/10.1038/nature02844
27. Beilstein K, Wittmann A, Grez M *et al.* Conditional control of mammalian gene expression by tetracycline-dependent hammerhead ribozymes. *ACS Synth Biol* 2015;4:526–34. https://doi.org/10.1021/sb500270h
28. Zhong G, Wang H, Bailey CC *et al.* Rational design of aptazyme riboswitches for efficient control of gene expression in mammalian cells. *eLife* 2016;5:18858. https://doi.org/10.7554/eLife.18858
29. Finke M, Brecht D, Stifel J *et al.* Efficient splicing-based RNA regulators for tetracycline-inducible gene expression in human cell culture and *C. elegans*. *Nucleic Acids Res* 2021;49:e71. https://doi.org/10.1093/nar/gkab233
30. Luo L, Jea JD-Y, Wang Y *et al.* Control of mammalian gene expression by modulation of polyA signal cleavage at 5′ UTR. *Nat Biotechnol* 2024;42:1454–66. https://doi.org/10.1038/s41587-023-01989-0
31. Fukunaga K, Dhamodharan V, Miyahira N *et al.* Small-molecule aptamer for regulating RNA functions in mammalian cells and animals. *J Am Chem Soc* 2023;145:7820–8. https://doi.org/10.1021/jacs.2c12332
32. Spöring M, Boneberg R, Hartig J. Aptamer-mediated control of polyadenylation for gene expression regulation in mammalian cells. *ACS Synth Biol* 2020;9:3008–18.
33. Weigand JE, Sanchez M, Gunnesch E-B *et al.* Screening for engineered neomycin riboswitches that control translation initiation. *RNA* 2008;14:89–97. https://doi.org/10.1261/rna.772408
34. Yu C-H, Luo J, Iwata-Reuyl D *et al.* Exploiting preQ1 riboswitches to regulate ribosomal frameshifting. *ACS Chem Biol* 2013;8:733–40. https://doi.org/10.1021/cb300629b
35. Ketzer P, Haas SF, Engelhardt S *et al.* Synthetic riboswitches for external regulation of genes transferred by replication-deficient

and oncolytic adenoviruses. *Nucleic Acids Res* 2012;40:e167. https://doi.org/10.1093/nar/gks734
36. Ketzer P, Kaufmann JK, Engelhardt S *et al.* Artificial riboswitches for gene expression and replication control of DNA and RNA viruses. *Proc Natl Acad Sci USA* 2014;111:554–62.
37. Tickner ZJ, Farzan M. Riboswitches for controlled expression of therapeutic transgenes delivered by adeno-associated viral vectors. *Pharmaceuticals* 2021;14:554. https://doi.org/10.3390/ph14060554
38. Lin Y-H, Chang K-Y. Rational design of a synthetic mammalian riboswitch as a ligand-responsive-1 ribosomal frame-shifting stimulator. *Nucleic Acids Res* 2016;44:9005–15. https://doi.org/10.1093/nar/gkw718
39. Regenthal R, Krueger M, Koeppel C *et al.* Drug levels: therapeutic and toxic serum/plasma concentrations of common drugs. *J Clin Monit Comput* 1999;15:529–44. https://doi.org/10.1023/A:1009935116877
40. Strobel B, Düchs MJ, Blazevic D *et al.* A small-molecule-responsive riboswitch enables conditional induction of viral vector-mediated gene expression in mice. *ACS Synth Biol* 2020;9:1292–305. https://doi.org/10.1021/acssynbio.9b00410
41. Berens C, Thain A, Schroeder R. A tetracycline-binding RNA aptamer. *Bioorg Med Chem* 2001;9:2549–56. https://doi.org/10.1016/S0968-0896(01)00063-3
42. Chopra I, Roberts M. Tetracycline antibiotics: mode of action, applications, molecular biology, and epidemiology of bacterial resistance. *Microbiol Mol Biol Rev* 2001;65:232–60. https://doi.org/10.1128/MMBR.65.2.232-260.2001
43. Müller M, Weigand JE, Weichenrieder O *et al.* Thermodynamic characterization of an engineered tetracycline-binding riboswitch. *Nucleic Acids Res* 2006;34:2607–17.
44. Weigand JE, Suess B. Tetracycline aptamer-controlled regulation of pre-mRNA splicing in yeast. *Nucleic Acids Res* 2007;35:4179–85. https://doi.org/10.1093/nar/gkm425
45. Agwuh KN, MacGowan A. Pharmacokinetics and pharmacodynamics of the tetracyclines including glycylcyclines. *J Antimicrob Chemother* 2006;58:256–65. https://doi.org/10.1093/jac/dkl224
46. Sano M, Nakasu A, Ohtaka M *et al.* A Sendai virus-based cytoplasmic RNA vector as a novel platform for long-term expression of microRNAs. *Mol Ther Methods Clin Dev* 2019;15:371–82. https://doi.org/10.1016/j.omtm.2019.10.012
47. Leber MF, Neault S, Jirovec E *et al.* Engineering and combining oncolytic measles virus for cancer therapy. *Cytokine Growth Factor Rev* 2020;56:39–48. https://doi.org/10.1016/j.cytogfr.2020.07.005
48. Wagner TE, Becraft JR, Bodner K *et al.* Small-molecule-based regulation of RNA-delivered circuits in mammalian cells. *Nat Chem Biol* 2018;14:1043–50. https://doi.org/10.1038/s41589-018-0146-9
49. Shao J, Li S, Qiu X *et al.* Engineered poly (A)-surrogates for translational regulation and therapeutic biocomputation in mammalian cells. *Cell Res* 2024;34:31–46. https://doi.org/10.1038/s41422-023-00896-y
50. Siu K-H, Chen W. Riboregulated toehold-gated gRNA for programmable CRISPR–Cas9 function. *Nat Chem Biol* 2019;15:217–20. https://doi.org/10.1038/s41589-018-0186-1
51. Jackson RJ, Hellen CU, Pestova TV. The mechanism of eukaryotic translation initiation and principles of its regulation. *Nat Rev Mol Cell Biol* 2010;11:113–27. https://doi.org/10.1038/nrm2838
52. Rodnina MV. Decoding and recoding of mRNA sequences by the ribosome. *Annu Rev Biophys* 2023;52:161–82. https://doi.org/10.1146/annurev-biophys-101922-072452
53. Gesteland RF, Atkins JF. Recoding: dynamic reprogramming of translation. *Annu Rev Biochem* 1996;65:741–68. https://doi.org/10.1146/annurev.bi.65.070196.003521
54. Gallant JA, Lindsley D. Leftward ribosome frameshifting at a hungry codon. *J Mol Biol* 1992;223:31–40. https://doi.org/10.1016/0022-2836(92)90713-T
55. Larsen B, Gesteland RF, Atkins JF. Structural probing and mutagenic analysis of the stem-loop required for *Escherichia coli* dnaX ribosomal frameshifting: programmed efficiency of 50%. *J Mol Biol* 1997;271:47–60. https://doi.org/10.1006/jmbi.1997.1162
56. Giedroc DP, Cornish PV. Frameshifting RNA pseudoknots: structure and mechanism. *Virus Res* 2009;139:193–208. https://doi.org/10.1016/j.virusres.2008.06.008
57. Plant EP, Jacobs KLM, Harger JW *et al.* The 9-Å solution: how mRNA pseudoknots promote efficient programmed −1 ribosomal frameshifting. *RNA* 2003;9:168–74. https://doi.org/10.1261/rna.2132503
58. Brierley I, Rolley NJ, Jenner AJ *et al.* Mutational analysis of the RNA pseudoknot component of a coronavirus ribosomal frameshifting signal. *J Mol Biol* 1991;220:889–902. https://doi.org/10.1016/0022-2836(91)90361-9
59. Caliskan N, Katunin VI, Belardinelli R *et al.* Programmed –1 frameshifting by kinetic partitioning during impeded translocation. *Cell* 2014;157:1619–31. https://doi.org/10.1016/j.cell.2014.04.041
60. Tsuchihashi Z, Kornberg A. Translational frameshifting generates the gamma subunit of DNA polymerase III holoenzyme. *Proc Natl Acad Sci USA* 1990;87:2516–20. https://doi.org/10.1073/pnas.87.7.2516
61. Chou M-Y, Lin S-C, Chang K-Y. Stimulation of −1 programmed ribosomal frameshifting by a metabolite-responsive RNA pseudoknot. *RNA* 2010;16:1236–44. https://doi.org/10.1261/rna.1922410
62. Hsu H-T, Lin Y-H, Chang K-Y. Synergetic regulation of translational reading-frame switch by ligand-responsive RNAs in mammalian cells. *Nucleic Acids Res* 2014;42:14070–82. https://doi.org/10.1093/nar/gku1233
63. Matsumoto S, Caliskan N, Rodnina MV *et al.* Small synthetic molecule-stabilized RNA pseudoknot as an activator for –1 ribosomal frameshifting. *Nucleic Acids Res* 2018;46:8079–89. https://doi.org/10.1093/nar/gky689
64. Xiao H, Edwards TE, Ferré-D'Amaré AR. Structural basis for specific, high-affinity tetracycline binding by an *in vitro* evolved aptamer and artificial riboswitch. *Chem Biol* 2008;15:1125–37. https://doi.org/10.1016/j.chembiol.2008.09.004
65. Penn WD, Mukhopadhyay S. Abracadabra, one becomes two: the importance of context in viral −1 programmed ribosomal frameshifting. *mBio* 2022;13:e0246821. https://doi.org/10.1128/mbio.02468-21
66. Matsumoto S, Caliskan N, Rodnina MV *et al.* Small synthetic molecule-stabilized RNA pseudoknot as an activator for –1 ribosomal frameshifting. *Nucleic Acids Res* 2018;46:8079–89. https://doi.org/10.1093/nar/gky689
67. Nelson ML, Levy SB. The history of the tetracyclines. *Ann NY Acad Sci* 2011;1241:17–32. https://doi.org/10.1111/j.1749-6632.2011.06354.x
68. Grossman TH. Tetracycline antibiotics and resistance. *Cold Spring Harb Perspect Med* 2016;6:a025387. https://doi.org/10.1101/cshperspect.a025387
69. Shutter MC, Akhondi H. Tetracycline. In: *StatPearls*, 2026, Treasure Island (FL), StatPearls Publishing. PMID: 31751095
70. Veinalde R, Grossardt C, Hartmann L *et al.* Oncolytic measles virus encoding interleukin-12 mediates potent antitumor effects through T cell activation. *OncoImmunology* 2017;6:e1285992. https://doi.org/10.1080/2162402X.2017.1285992
71. Chassin H, Müller M, Tigges M *et al.* A modular degron library for synthetic circuits in mammalian cells. *Nat Commun* 2019;10:2013.
72. Harger JW, Dinman JD. An *in vivo* dual-luciferase assay system for studying translational recoding in the yeast *Saccharomyces*

cerevisiae. *RNA* 2003;9:1019–24. https://doi.org/10.1261/rna.5930803
73. Grentzmann G, Ingram JA, Kelly PJ *et al.* A dual-luciferase reporter system for studying recoding signals. *RNA* 1998;4:479–86.
74. Bhatt PR, Scaiola A, Loughran G *et al.* Structural basis of ribosomal frameshifting during translation of the SARS-CoV-2 RNA genome. *Science* 2021;372:1306–13. https://doi.org/10.1126/science.abf3546
75. Finch LK, Ling R, Napthine S *et al.* Characterization of ribosomal frameshifting in Theiler's murine encephalomyelitis virus. *J Virol* 2015;89:8580–9. https://doi.org/10.1128/JVI.01043-15
76. Dulude D, Baril M, Brakier-Gingras L. Characterization of the frameshift stimulatory signal controlling a programmed –1 ribosomal frameshift in the human immunodeficiency virus type 1. *Nucleic Acids Res* 2002;30:5094–102. https://doi.org/10.1093/nar/gkf657
77. Staple DW, Butcher SE. Solution structure of the HIV-1 frameshift inducing stem–loop RNA. *Nucleic Acids Res* 2003;31:4326–31. https://doi.org/10.1093/nar/gkg654
78. Brakier-Gingras L, Charbonneau J, Butcher SE. Targeting frameshifting in the human immunodeficiency virus. *Expert Opin Ther Targets* 2012;16:249–58. https://doi.org/10.1517/14728222.2012.665879
79. Dinman JD, Richter S, Plant EP *et al.* The frameshift signal of HIV-1 involves a potential intramolecular triplex RNA structure. *Proc Natl Acad Sci USA* 2002;99:5331–6. https://doi.org/10.1073/pnas.082102199
80. Rodnina MV, Korniy N, Klimova M *et al.* Translational recoding: canonical translation mechanisms reinterpreted. *Nucleic Acids Res* 2020;48:1056–67. https://doi.org/10.1093/nar/gkz783
81. Lin Z, Gilbert RJ, Brierley I. Spacer-length dependence of programmed −1 or −2 ribosomal frameshifting on a U 6 A heptamer supports a role for messenger RNA (mRNA) tension in frameshifting. *Nucleic Acids Res* 2012;40:8674–89. https://doi.org/10.1093/nar/gks629
82. Brierley I, Jenner AJ, Inglis SC. Mutational analysis of the "slippery-sequence" component of a coronavirus ribosomal frameshifting signal. *J Mol Biol* 1992;227:463–79. https://doi.org/10.1016/0022-2836(92)90901-U
83. Napthine S, Liphardt J, Bloys A *et al.* The role of RNA pseudoknot stem 1 length in the promotion of efficient −1 ribosomal frameshifting. *J Mol Biol* 1999;288:305–20. https://doi.org/10.1006/jmbi.1999.2688
84. Mouzakis KD, Lang AL, Vander Meulen KA *et al.* HIV-1 frameshift efficiency is primarily determined by the stability of base pairs positioned at the mRNA entrance channel of the ribosome. *Nucleic Acids Res* 2013;41:1901–13. https://doi.org/10.1093/nar/gks1254
85. Lin Z, Gilbert RJC, Brierley I. Spacer-length dependence of programmed −1 or −2 ribosomal frameshifting on a U 6 A heptamer supports a role for messenger RNA (mRNA) tension in frameshifting. *Nucleic Acids Res* 2012;40:8674–89. https://doi.org/10.1093/nar/gks629
86. Plant EP, Dinman JD. Comparative study of the effects of heptameric slippery site composition on −1 frameshifting among different eukaryotic systems. *RNA* 2006;12:666–73. https://doi.org/10.1261/rna.2225206
87. Liu Z, Chen O, Wall JBJ *et al.* Systematic comparison of 2A peptides for cloning multi-genes in a polycistronic vector. *Sci Rep* 2017;7:2193. https://doi.org/10.1038/s41598-017-02460-2
88. Donnelly ML, Luke G, Mehrotra A *et al.* Analysis of the aphthovirus 2A/2B polyprotein 'cleavage'mechanism indicates not a proteolytic reaction, but a novel translational effect: a putative ribosomal 'skip'. *J Gen Virol* 2001;82:1013–25. https://doi.org/10.1099/0022-1317-82-5-1013
89. Szymczak AL, Vignali DA. Development of 2A peptide-based strategies in the design of multicistronic vectors. *Expert Opin Biol Ther* 2005;5:627–38. https://doi.org/10.1517/14712598.5.5.627
90. Zhu X, Ricci-Tam C, Hager ER *et al.* Self-cleaving peptides for expression of multiple genes in *Dictyostelium discoideum*. *PLoS One* 2023;18:0281211.
91. Matentzoglu K, Scheffner M. Ubiquitin-fusion protein system: a powerful tool for ectopic protein expression in mammalian cells. *BioTechniques* 2009;46:21–8. https://doi.org/10.2144/000113023
92. Hondred D, Walker JM, Mathews DE *et al.* Use of ubiquitin fusions to augment protein expression in transgenic plants. *Plant Physiol* 1999;119:713–24. https://doi.org/10.1104/pp.119.2.713
93. Finley D, Sadis S, Monia BP *et al.* Inhibition of proteolysis and cell cycle progression in a multiubiquitination-deficient yeast mutant. *Mol Cell Biol* 1994;14:5501–9.
94. Loughran G, Andreev DE, Terenin IM *et al.* Guidelines for minimal reporting requirements, design and interpretation of experiments involving the use of eukaryotic dual gene expression reporters (MINDR). *Nat Struct Mol Biol* 2025;32:418–30.
95. Loughran G, Howard MT, Firth AE *et al.* Avoidance of reporter assay distortions from fused dual reporters. *RNA* 2017;23:1285–9. https://doi.org/10.1261/rna.061051.117
96. Close DM, Hahn RE, Patterson SS *et al.* Comparison of human optimized bacterial luciferase, firefly luciferase, and green fluorescent protein for continuous imaging of cell culture and animal models. *J Biomed Opt* 2011;16:047003–10. https://doi.org/10.1117/1.3564910
97. Fan F, Wood KV. Bioluminescent assays for high-throughput screening. *Assay Drug Dev Technol* 2007;5:127–36. https://doi.org/10.1089/adt.2006.053
98. Trinchieri G, Pflanz S, Kastelein RA. The IL-12 family of heterodimeric cytokines: new players in the regulation of T cell responses. *Immunity* 2003;19:641–4. https://doi.org/10.1016/S1074-7613(03)00296-6
99. Nguyen KG, Vrabel MR, Mantooth SM, Hopkins JJ, Wagner ES, Gabaldon TA, Zaharoff DA, Localized Interleukin-12 for Cancer Immunotherapy.. *Front Immunol* 2020;11:575597.
100. Hsieh C-S, Macatonia SE, Tripp CS *et al.* Development of TH1 CD4+ T cells through IL-12 produced by *Listeria*-induced macrophages. *Science* 1993;260:547–9. https://doi.org/10.1126/science.8097338
101. Trinchieri G. Interleukin-12: a proinflammatory cytokine with immunoregulatory functions that bridge innate resistance and antigen-specific adaptive immunity. *Annu Rev Immunol* 1995;13:251–76. https://doi.org/10.1146/annurev.iy.13.040195.001343
102. Leonard JP, Sherman ML, Fisher GL *et al.* Effects of single-dose interleukin-12 exposure on interleukin-12–associated toxicity and interferon-γ production. *Blood* 1997;90:2541–8.
103. Vanrell L, Scala M, Blanco L *et al.* Development of a liver-specific Tet-on inducible system for AAV vectors and its application in the treatment of liver cancer. *Mol Ther* 2011;19:1245–53. https://doi.org/10.1038/mt.2011.37
104. Barrett JA, Cai H, Miao J *et al.* Regulated intratumoral expression of IL-12 using a RheoSwitch Therapeutic System®(RTS®) gene switch as gene therapy for the treatment of glioma. *Cancer Gene Ther* 2018;25:106–16. https://doi.org/10.1038/s41417-018-0019-0
105. Düchs MJ, Kratzer RF, Vieyra-Garcia P *et al.* Riboswitch-controlled IL-12 gene therapy reduces hepatocellular cancer in mice. *Front Immunol* 2024;15:1360063.
106. Wilusz JE, JnBaptiste CK, Lu LY *et al.* A triple helix stabilizes the 3′ ends of long noncoding RNAs that lack poly (A) tails. *Genes Dev* 2012;26:2392–407. https://doi.org/10.1101/gad.204438.112
107. Brown JA, Bulkley D, Wang J *et al.* Structural insights into the stabilization of MALAT1 noncoding RNA by a bipartite triple

helix. *Nat Struct Mol Biol* 2014;21:633–40. https://doi.org/10.1038/nsmb.2844
108. Chadalavada DM, Senchak SE, Bevilacqua PC. The folding pathway of the genomic hepatitis delta virus ribozyme is dominated by slow folding of the pseudoknots. *J Mol Biol* 2002;317:559–75. https://doi.org/10.1006/jmbi.2002.5434
109. Brown JA, Valenstein ML, Yario TA *et al.* Formation of triple-helical structures by the 3′-end sequences of MALAT1 and MENβ noncoding RNAs. *Proc Natl Acad Sci USA* 2012;109:19202–7. https://doi.org/10.1073/pnas.1217338109
110. Walker SC, Avis JM, Conn GL. General plasmids for producing RNA *in vitro* transcripts with homogeneous ends. *Nucleic Acids Res* 2003;31:e82. https://doi.org/10.1093/nar/gng082
111. Hill CH, Brierley I. Structural and functional insights into viral programmed ribosomal frameshifting. *Annu Rev Virol* 2023;10:217–42. https://doi.org/10.1146/annurev-virology-111821-120646
112. Atkins JF, Loughran G, Bhatt PR *et al.* Ribosomal frameshifting and transcriptional slippage: from genetic steganography and cryptography to adventitious use. *Nucleic Acids Res* 2016;44:7007–78.
113. Dinman JD. Translational recoding signals: expanding the synthetic biology toolbox. *J Biol Chem* 2019;294:7537–45. https://doi.org/10.1074/jbc.REV119.006348
114. Riegger RJ, Caliskan N. Thinking outside the frame: impacting genomes capacity by programmed ribosomal frameshifting. *Front Mol Biosci* 2022;9:842261. https://doi.org/10.3389/fmolb.2022.842261
115. Caliskan N, Peske F, Rodnina MV. Changed in translation: mRNA recoding by −1 programmed ribosomal frameshifting. *Trends Biochem Sci* 2015;40:265–74. https://doi.org/10.1016/j.tibs.2015.03.006
116. Wachsmuth M, Findeiß S, Weissheimer N *et al. De novo* design of a synthetic riboswitch that regulates transcription termination. *Nucleic Acids Res* 2013;41:2541–51. https://doi.org/10.1093/nar/gks1330
117. Olenginski LT, Spradlin SF, Batey RT. Flipping the script: understanding riboswitches from an alternative perspective. *J Biol Chem* 2024;300:105730. https://doi.org/10.1016/j.jbc.2024.105730
118. Ciano-Petersen NL, Muñiz-Castrillo S, Birzu C *et al.* Cytokine dynamics and targeted immunotherapies in autoimmune encephalitis. *Brain Commun* 2022;4:196. https://doi.org/10.1093/braincomms/fcac196
119. Yi M, Li T, Niu M *et al.* Targeting cytokine and chemokine signaling pathways for cancer therapy. *Sig Transduct Target Ther* 2024;9:176. https://doi.org/10.1038/s41392-024-01868-3
120. Mustafina K, Nomura Y, Rotrattanadumrong R *et al.* Circularly-permuted pistol ribozyme: a synthetic ribozyme scaffold for mammalian riboswitches. *ACS Synth Biol* 2021;10:2040–8. https://doi.org/10.1021/acssynbio.1c00213
121. Stifel J, Spöring M, Hartig JS. Expanding the toolbox of synthetic riboswitches with guanine-dependent aptazymes. *Synth Biol (Oxf)* 2019;4:ysy022. https://doi.org/10.1093/synbio/ysy022
122. Mustafina K, Fukunaga K, Yokobayashi Y. Design of mammalian ON-riboswitches based on tandemly fused aptamer and ribozyme. *ACS Synth Biol* 2020;9:19–25. https://doi.org/10.1021/acssynbio.9b00371
123. Strobel B, Spöring M, Klein H *et al.* High-throughput identification of synthetic riboswitches by barcode-free amplicon-sequencing in human cells. *Nat Commun* 2020;11:714. https://doi.org/10.1038/s41467-020-14491-x
124. Pu Q, Zhou S, Huang X *et al.* Intracellular selection of theophylline-sensitive hammerhead aptazyme. *Molecular Therapy Nucleic Acids* 2020;20:400–8. https://doi.org/10.1016/j.omtn.2020.03.001

Received: September 8, 2025. **Revised:** March 31, 2026. **Accepted:** April 15, 2026